LETTER

doi:10.1038/nature13561

PRC2 loss amplifies Ras-driven transcription and confers sensitivity to BRD4-based therapies

Thomas De Raedt[1,2,3], Eline Beert[4]*†, Eric Pasmant[5,6]*, Armelle Luscan[5,6], Hilde Brems[4], Nicolas Ortonne[5,6], Kristian Helin[7,8,9], Jason L. Hornick[10], Victor Mautner[11], Hildegard Kehrer-Sawatzki[12], Wade Clapp[13], James Bradner[2,14], Michel Vidaud[5,6], Meena Upadhyaya[15], Eric Legius[4,16] & Karen Cichowski[1,2,3]

The polycomb repressive complex 2 (PRC2) exerts oncogenic effects in many tumour types[1]. However, loss-of-function mutations in PRC2 components occur in a subset of haematopoietic malignancies, suggesting that this complex plays a dichotomous and poorly understood role in cancer[2,3]. Here we provide genomic, cellular, and mouse modelling data demonstrating that the polycomb group gene *SUZ12* functions as tumour suppressor in PNS tumours, high-grade gliomas and melanomas by cooperating with mutations in *NF1*. *NF1* encodes a Ras GTPase-activating protein (RasGAP) and its loss drives cancer by activating Ras[4]. We show that *SUZ12* loss potentiates the effects of *NF1* mutations by amplifying Ras-driven transcription through effects on chromatin. Importantly, however, *SUZ12* inactivation also triggers an epigenetic switch that sensitizes these cancers to bromodomain inhibitors. Collectively, these studies not only reveal an unexpected connection between the PRC2 complex, *NF1* and Ras, but also identify a promising epigenetic-based therapeutic strategy that may be exploited for a variety of cancers.

The Ras pathway is commonly deregulated in cancer[5]. Oncogenic *RAS* mutations occur in approximately 30% of tumours; however, mutations in upstream regulators and downstream effectors are also prevalent[5]. Irrespective of aetiology, the oncogenic Ras signal is frequently potentiated as cancers progress, in some instances through amplification of mutant *RAS* genes or suppression of negative feedback pathways[6–9]. It is likely that many unknown mechanisms contribute to this emerging aspect of tumour evolution.

Mutations in RasGAP genes promote Ras activation in many cancers[4,10,11]. Defects in the *NF1* RasGAP underlie a familial cancer syndrome (NF1), sporadic glioblastomas (GBMs), neuroblastomas and lung cancer[4]. Interestingly, some severely affected patients with NF1 (NF1 microdeletion patients) carry germline deletions of *NF1* and 13 surrounding genes[12,13]. These individuals develop thousands of benign tumours and can exhibit a fourfold increased risk of malignancies[14,15], suggesting that a cooperating tumour suppressor lies within this region. If true, this gene might affect the development of tumours in patients with NF1 and in sporadic cancers, which frequently possess large 17q deletions[16]. Therefore, we analysed 51 malignant peripheral nerve sheath tumours (MPNSTs), the most common NF1-associated malignancy, from patients with and without an NF1 microdeletion. Array comparative genomic hybridization revealed heterozygous and homozygous deletions of *SUZ12*, a gene within the microdeletion, which encodes a component of the PRC2 (Fig. 1a, Extended Data Fig. 1a and Extended Data Table 1). Deletions in *EED*, another PRC2 component, were also prevalent in both populations. Moreover, inactivating mutations in *SUZ12* and *EED* were frequently present (Fig. 1a, Extended Data Fig. 1b, c and Supplementary Information). Together, 79% of microdeletion and 34% of non-microdeletion tumours exhibited homozygous loss of *SUZ12* or *EED*; however, 53% of non-microdeletion MPNSTs harboured one or more PRC2 mutations/deletions (Fig. 1b). These observations suggest that PRC2 inactivation may play a critical role in MPNST development.

SUZ12 and H3K27me3 were undetectable in primary MPNSTs harbouring *SUZ12* mutations and in four *NF1*-deficient human MPNST cell lines (Extended Data Fig. 1d, e and Fig. 1c). *SUZ12* reconstitution restored H3K27me3, reduced proliferation and triggered cell death in low serum (Fig. 1c, d and Extended Data 1f). The *SUZ12* lentivirus did not affect *SUZ12* wild-type cells (Extended Data Fig. 1g). Conversely, *SUZ12* ablation enhanced colony growth of *NF1*-deficient (U251 (ref. 17)) but not *NF1* wild-type GBM cells (Fig. 1e and Extended Data Fig. 1h). Partly effective short hairpin RNAs (shRNAs) exerted a disproportionate suppressive effect on H3K27Me3 and promoted colony growth of U251 cells, albeit less efficiently (Fig. 1e). These results suggest that reduced PRC2 dosage might also contribute to tumour development, which could be relevant in the setting of heterozygous *SUZ12*/*EED* mutations (Fig. 1b). Finally, *SUZ12* ablation enhanced colony growth of *NF1*-deficient but not *NF1* wild-type melanoma cells (Fig. 1f and Extended Data Fig. 1i).

To assess the cooperativity of these genes further, $Nf1^{+/-}$; $Suz12^{+/-}$ '*cis*' mice, carrying mutations on the same chromosome, were generated to recapitulate the genetics of microdeletion patients and spontaneous tumours. Tumours in *Nf1* mouse models are driven by spontaneous loss of wild-type chromosome 11 (ref. 18), resulting in *Nf1* and *Suz12* loss (Extended Data Fig. 2a). $Nf1^{+/-}$; $Suz12^{+/-}$ mice were highly tumour prone and exhibited decreased survival (Fig. 2a). Notably, mice developed lesions associated with both germline and spontaneous *NF1* mutations in humans, including neurofibromas, MPNSTs, schwannomas, melanocytic nevi and intestinal adenomas (Fig. 2b and Extended Data Fig. 2b)[4]. Genomic human tumour data demonstrate that at least one allele of *NF1* and *SUZ12* are co-deleted/mutated in 24% of melanomas (Fig. 2c). Moreover, *EED* deletions/mutations are present in 44% of *NF1*-mutant tumours, most of which also lack one *SUZ12* allele.

To investigate *SUZ12* in MPNST development further, mice harbouring *cis* mutations in *Nf1*, *p53* and *Suz12* were also generated, as combined *NF1*/*p53* mutations drive MPNST formation[18–20] (Supplementary Information). These *Nf1*/*p53*/*Suz12* mice exhibited decreased survival and developed MPNSTs on average 2.3 months earlier than *Nf1*/*p53* mutant

[1]Genetics Division, Department of Medicine, Brigham and Women's Hospital, Boston, Massachusetts 02115, USA. [2]Harvard Medical School, Boston, Massachusetts 02115, USA. [3]Ludwig Center at Dana-Farber/Harvard Cancer Center, Boston, Massachusetts 02115, USA. [4]Department of Human Genetics, Catholic University Leuven, 3000 Leuven, Belgium. [5]INSERM UMR_S745 et EA7331, Université Paris Descartes, Sorbonne Paris Cité, Faculté des Sciences Pharmaceutiques et Biologiques, 75006 Paris, France. [6]Service de Biochimie et Génétique Moléculaire, Hôpital Cochin, Assistance Publique-Hôpitaux de Paris, 75014 Paris, France. [7]Biotech Research and Innovation Centre (BRIC), University of Copenhagen, 2200 Copenhagen, Denmark. [8]Center for Epigenetics, University of Copenhagen, 2200 Copenhagen, Denmark. [9]The Danish Stem Cell Center (Danstem), University of Copenhagen, 2200 Copenhagen, Denmark. [10]Department of Pathology, Brigham and Women's Hospital, Boston, Massachusetts 02115, USA. [11]Department of Maxillofacial Surgery, University Medical Centre, Hamburg-Eppendorf, 20246 Hamburg, Germany. [12]Institute of Human Genetics, University of Ulm, 89081 Ulm, Germany. [13]Herman Wells Center for Pediatric Research, Department of Pediatrics, Indiana University School of Medicine, 46202 Indianapolis, Indiana, USA. [14]Department of Medical Oncology, Dana-Farber Cancer Institute, Massachusetts 02115, USA. [15]Institute of Medical Genetics, Cardiff University, Heath Park, Cardiff CF14 4XN, UK. [16]Center for Human Genetics, University Hospital Leuven, 3000 Leuven Belgium. †Present address: Laboratory of Aquatic Biology, Interdisciplinary Research Facility Life Sciences, Katholieke Universiteit, Leuven Afdeling Kortrijk, 8500 Kortrijk, Belgium.
*These authors contributed equally to this work.

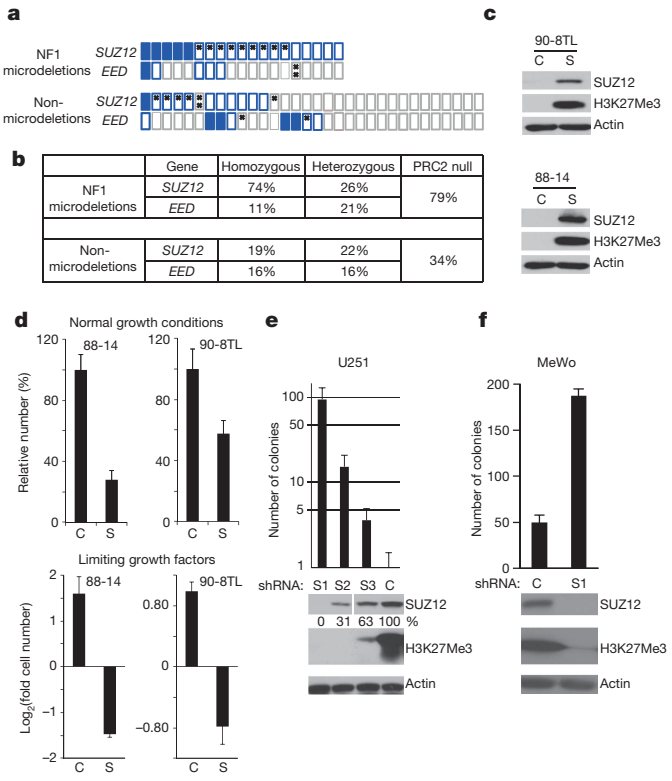

Figure 1 | PRC2 components are deleted or mutated in human MPNSTs and exert tumour-suppressive activity. **a**, Schematic visualization of distinct genomic alterations in *SUZ12* and *EED* in *NF1*-deficient human MPNSTs from patients with and without an NF1 microdeletion (asterisk, mutation; open blue rectangle, hemizygous deletion; filled blue rectangle, homozygous deletion; grey rectangle, no copy number loss). **b**, Table indicating the percentage of human MPNSTs with homozygous or heterozygous loss of *SUZ12*, *EED* and *PRC2*. **c**, Immunoblots of lysates from human MPNST cells reconstituted with *SUZ12* (C, LacZ control; S, *SUZ12*). Restoration of H3K27me3 shows that the functionality of the PRC2 complex is restored upon *SUZ12* reconstitution. **d**, Human MPNST cell lines with reconstituted *SUZ12* exhibit reduced proliferation under normal growth conditions (10% serum, 3 days). *SUZ12* reconstitution (S) causes cell death when cells are cultured under limiting growth factors (2% serum, 6 days). Proliferation curves are shown in Extended Data Fig. 1f. **e**, Top, graph depicting colony growth in soft agar using the *NF1*-deficient human GBM line (U251), expressing a control shRNA construct (C, short hairpin green fluorescent protein (shGFP)) or three distinct SUZ12 shRNA constructs against SUZ12 (S1–S3). Bottom, immunoblots depicting knockdown of SUZ12 to varying levels (S1–S3) compared with control (shGFP). The percentage of SUZ12 remaining is quantified. **f**, Effects of shSUZ12 (S1) on SUZ12 expression and colony formation in MEWO melanoma cells, which are *NF1* null. Error bars, s.d. ($n = 3$, biological replicates).

mice (Fig. 2d, e). All MPNSTs arose in less than 3.5 months, whereas MPNSTs in *Nf1/p53* mice required up to 9 months. Nevertheless, fewer *Nf1/p53/Suz12* animals developed MPNSTs, most probably because of the increase in other tumour types (Fig. 2f). Strikingly, 54% of *Nf1/p53/Suz12* mice developed high-grade gliomas and did so on average in approximately 3 months, a latency shorter than most models (Fig. 2e, f and Extended Data Fig. 2d). *NF1* and *SUZ12* were co-deleted/mutated in 14% of human GBMs (Fig. 2g). *EED* deletions were also detected in 26% of *NF1*-mutant tumours, which all lacked a copy of *SUZ12*, highlighting the co-occurrence of defects in *NF1* and PRC2.

SUZ12 ablation causes a loss of H3K27me3 and in some settings promotes a consequential increase in H3K27Ac[21]: a transcriptional activating signal that recruits bromodomain proteins and associated transcription factors[22]. As such, we reasoned that *SUZ12*-mutant MPNSTs might be sensitive to bromodomain inhibitors such as JQ1[23]. Importantly, *SUZ12* reconstitution increased H3K27me3 and decreased H3K27Ac in MPNST

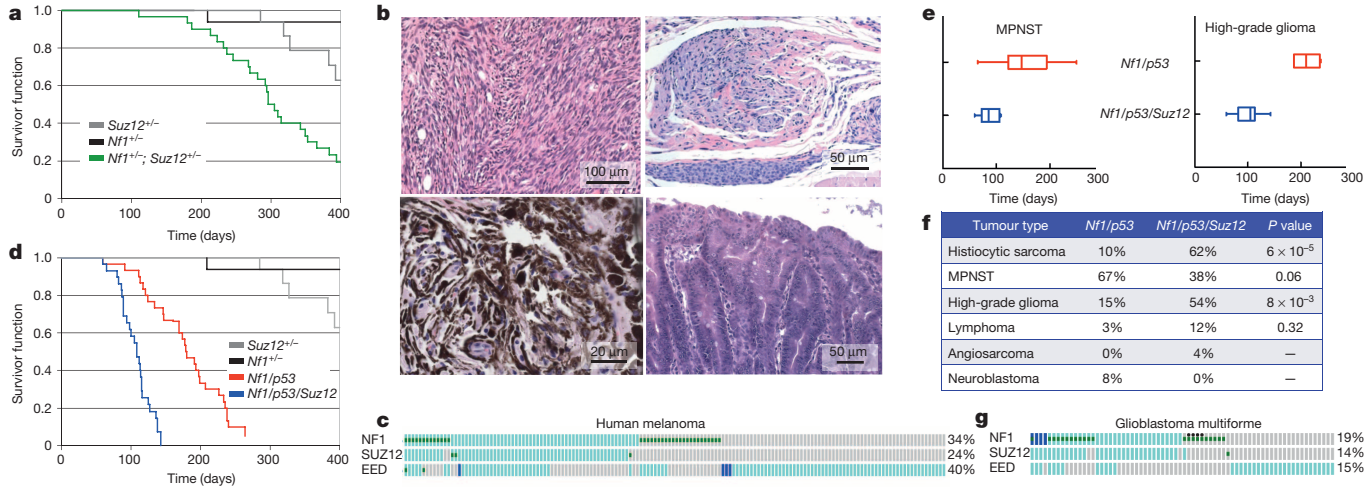

Figure 2 | *Suz12* and *Nf1* mutations cooperate to promote widespread tumour development in mice. **a**, Kaplan–Meier curve comparing survival of $Suz12^{+/-}$ ($n = 15$), $Nf1^{+/-}$ ($n = 15$) and $Nf1^{+/-}$; $Suz12^{+/-}$ ($n = 30$) mice in *cis* ($NS^{+/-}$). $Nf1^{+/-}$; $Suz12^{+/-}$ mice have a significantly reduced survival ($Nf1^{+/-}$; $Suz12^{+/-}$ versus $Suz12^{+/-}$, $P = 1.99 \times 10^{-4}$; $Nf1^{+/-}$; $Suz12^{+/-}$ versus $Nf1^{+/-}$, $P = 2.87 \times 10^{-8}$; Mantel–Cox test). **b**, Haematoxylin and eosin staining of an MPNST (top left), neurofibroma (top right), melanocytic nevus (bottom left) and intestinal adenoma (bottom right) in $Nf1^{+/-}$; $Suz12^{+/-}$ mice. **c**, Oncoprint output of the melanoma TCGA data (cBioPortal) (green square, mutation; light blue rectangle, hemizygous deletion; dark blue rectangle, homozygous deletion; grey rectangle, unaltered). **d**, Kaplan–Meier curve comparing survival of $Suz12^{+/-}$, $Nf1^{+/-}$, $Nf1^{+/-}/p53^{+/-}$ mice ($n = 30$) in *cis* ($NP^{+/-}$) and $Nf1^{+/-}$ $p53^{+/-}$ $Suz12^{+/-}$ mice in *cis* ($NPS^{+/-}$). *Nf1/p53/Suz12* mice have a significantly lower survival ($P = 1.2 \times 10^{-9}$, Mantel–Cox test). **e**, Left, box plot comparing the age at onset for MPNSTs in *Nf1/p53* and *Nf1/p53/Suz12* mice. MPNSTs from *Nf1/p53/Suz12* mice have a significantly shorter latency (on average 2.3 months; $P = 2.8 \times 10^{-4}$, Mann–Whitney *U*-test). Right, box plot comparing the age at onset for high-grade glioma in *Nf1/p53* and *Nf1/p53/Suz12* mice. High-grade gliomas in *Nf1/p53/Suz12* mice develop on average around 3 months and have a significantly shorter latency ($P = 0.0003$, Mann–Whitney *U*-test). **f**, Table comparing the percentages of *Nf1/p53* and *Nf1/p53/Suz12* mice that develop specific tumours. *P* values indicate significance by Fisher's exact test. **g**, Oncoprint output of the glioblastoma TCGA data (cBioPortal) (green square, mutation; light blue rectangle, hemizygous deletion; dark blue rectangle, homozygous deletion; black dot, second hit mutation). Co-occurrence of defects in *NF1* and the PRC2 complex (NF1–SUZ12, odds ratio >10, $P < 10^{-4}$; NF1–EED, odds ratio 2–10, $P = 2.2 \times 10^{-4}$).

cells, whereas *SUZ12* ablation decreased H3K27me3 and increased H3K27Ac (Fig. 3a). Moreover, *SUZ12*-deficient MPNSTs were more sensitive to JQ1 than PRC2 wild-type cells (Fig. 3b).

Transcriptional profiling analysis was conducted in MPNSTs, in the presence/absence of *SUZ12* or JQ1. Gene set enrichment analysis (GSEA) and single-sample (ss)GSEA demonstrated that the gene set suppressed by *SUZ12* was also suppressed by JQ1 (Supplementary Table 1 and Fig. 3c). Using the Molecular Signatures Database we found that PRC2-regulated genes were suppressed both in *SUZ12*-reconstituted and JQ1-treated cells, suggesting that JQ1 counteracts *SUZ12* loss, in part, by repressing PRC2 targets (Extended data Fig. 3a, b). Unlike other tumours, neither JQ1 nor *SUZ12* suppressed *MYC* genes (Extended Data Fig. 3c). However, *MYC* genes are not upregulated and do not drive MPNST development. Surprisingly, *SUZ12* and JQ1 also suppressed genes associated with oncogenic Ras transcriptional signatures (Fig. 3d and Extended Data Fig. 3a). Conversely, Ras signatures were enhanced when *SUZ12* was ablated in *NF1*-mutant GBM cells (Fig. 3d). Phospho-ERK was unaffected by *SUZ12* loss, reconstitution, or JQ1 treatment (Extended Data Fig. 3d), suggesting that *SUZ12* loss amplifies Ras transcriptional output via direct effects on chromatin, and that JQ1 may counteract effects by suppressing Ras signature genes.

There are no effective therapies for MPNSTs[24]. While *SUZ12*-mutant MPNSTs were sensitive to JQ1, in contrast to c-Myc driven tumours, the effects were cytostatic[25,26]. Given the importance of Ras in MPNSTs, we investigated whether JQ1 might cooperate with Ras pathway inhibitors.

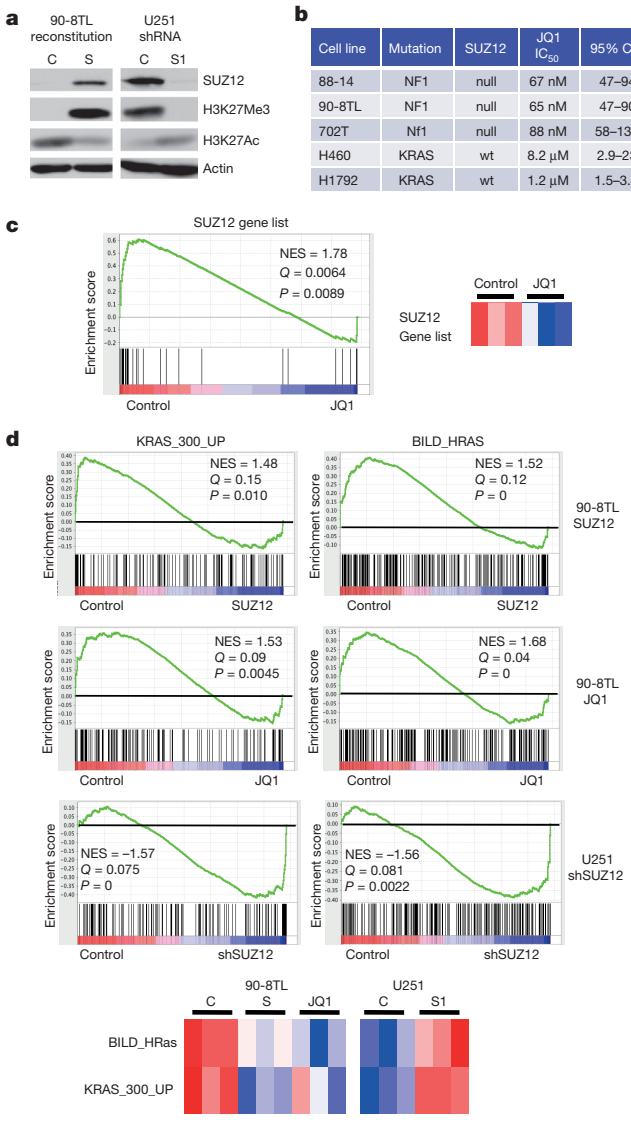

Cell line	Mutation	SUZ12	JQ1 IC_{50}	95% CI
88-14	NF1	null	67 nM	47–94
90-8TL	NF1	null	65 nM	47–90
702T	Nf1	null	88 nM	58–133
H460	KRAS	wt	8.2 μM	2.9–23
H1792	KRAS	wt	1.2 μM	1.5–3.4

JQ1 was evaluated in combination with an mTOR inhibitor (rapamycin), or a MEK inhibitor (PD-901) as both effectors function in *NF1*-deficient tumours[27–30]. Only PD-901/JQ1 treatment killed MPNSTs (Fig. 4a). Genetic ablation of BRD4 similarly cooperated with PD-901 (Extended Data Fig. 4a, b). *SUZ12* suppression conferred sensitivity to PD-901/JQ1 in other *NF1*-deficient tumour cells, including GBM and colon cancer, whereas *SUZ12* suppression did not affect *NF1* wild-type cells (Extended Data Fig. 4c and Supplementary Information).

To elucidate the cooperativity between BRD4 and MEK inhibitors, transcriptional profiling and chromatin immunoprecipitation followed by sequencing (ChIP-seq) experiments were performed. We compiled a list of publicly available upregulated Ras signature genes significantly repressed by JQ1, PD-901 or JQ1/PD901 in MPNSTs (Supplementary Table 2 and Supplementary Information). PD-901 suppressed a high percentage (58%) of these Ras signature genes (Fig. 4b, blue boxes) and JQ1 suppressed 29% (yellow boxes). However, JQ1/PD-901 cooperated to suppress this Ras signature in several ways. Not only did JQ1 suppress genes unaffected by PD-901, but the JQ1/PD-901 combination enhanced or uniquely suppressed 26% of these genes (green boxes). ssGSEA of our Ras signature gene set confirmed the cooperative effects of PD901 and JQ1 (Fig. 4c). H3K27Ac and BRD4 were significantly enriched at promoters of JQ1/PD-901 suppressed targets (Fig. 4b, red boxes) and BRD4 was displaced at 53% of sites (red boxes with dots), as shown in Fig. 4d. Transcription factors including ETS1, a known master regulator of Ras-driven transcription, were suppressed by JQ1/PD-901.

Finally, PD-901 and JQ1 were evaluated in *Nf1/p53/Suz12* mice (Fig. 4e). PD-901 did not affect MPNSTs, whereas JQ1 exerted modest, cytostatic effects. However, combined JQ1/PD-901 triggered significant tumour regression. On average, tumours shrank 67%; however, half of them shrank by at least 75%. On the basis of their mechanism of development, tumours from *Nf1/p53* mice are *SUZ12* heterozygous, recapitulating an additional subset of human tumours (Fig. 1b). Consistent with shRNA studies (Fig. 1e), tissue from $Suz12^{+/-}$ mice revealed a disproportionate loss of H3K27me3 (Fig. 4f), potentially conferring sensitivity to PD-901/JQ1. Indeed, $Nf1^{-/-}$;$p53^{-/-}$;$Suz12^{+/-}$ tumours shrank up to 68% (Fig. 4g), albeit overall less than tumours in *Nf1/p53/Suz12* mice. Notably, H3K27me3 antibodies faithfully detected PRC2 defects in primary human tumours (Fig. 4h, Extended Data Fig. 4d and

Figure 3 | SUZ12 and JQ1 regulate PRC2 targets and the Ras transcriptional signature. a, Left, immunoblots showing the epigenetic switch from H3K27Ac to H3K27Me3 upon *SUZ12* reconstitution in human 90-8TL MPNST cells (C, LacZ; S, *SUZ12* reconstitution; H3K27Me3 expression included here with immunoblots is also shown in Fig. 1c). Right, epigenetic switch from H3K27Me3 to H3K27Ac upon *SUZ12* knockdown in *NF1*-deficient GBMs (U251) (C, scramble shRNA; S1, SUZ12 shRNA). **b**, Half-maximum inhibitory concentration (IC_{50}) values of JQ1 in cell lines null and wild type (WT) for *SUZ12* and *NF1* as indicated. 702T cells are *Nf1/p53/suz12* null MPNSTs derived from our mouse tumours. *KRAS* mutant/*SUZ12* WT H460 and H1792 lung cancer lines were used as a comparison. 95% CI, 95% confidence interval. **c**, Top, signature enrichment plot comparing the SUZ12 signature (genes downregulated in response to SUZ12 reconstitution; Supplementary Table 1) in MPNST cells treated with vehicle versus JQ1 (100 nM, 24 h, triplicate samples). Plot indicates that SUZ12-regulated genes are more highly expressed in control than JQ1-treated samples (red, upregulation; blue, downregulation). NES, normalized enrichment score. Bottom, heat map of the enrichment scores of SUZ12 downregulated genes in vehicle (control) and JQ1 (three replicates) (red, upregulation; blue, downregulation). **d**, Top, Ras signature enrichment plots (using KRAS_300_UP.V1_UP and BILD_HRAS signature data sets obtained from the Molecular Signatures Database) in MPNSTs (90-8TL) reconstituted with SUZ12 versus control vector or treatment with JQ1 versus vehicle control (100 nM, 24 h, triplicate samples) and in the human GBM line U251 after knockdown of SUZ12 (shSUZ12 S1). Plots indicate a significant downregulation of RAS signatures after SUZ12 reconstitution and JQ1 treatment, and a significant upregulation of RAS signatures in *SUZ12*-depleted cells. Bottom, heat map of the enrichment scores of Ras signatures in control (C, LacZ), *SUZ12*-reconstituted (S) and JQ1-treated MPNST cells (three replicates), and in control (C, *shScamble*) and SUZ12-ablated (S1, *shSUZ12*) U251 cells (three replicates) (red, upregulation; blue, downregulation).

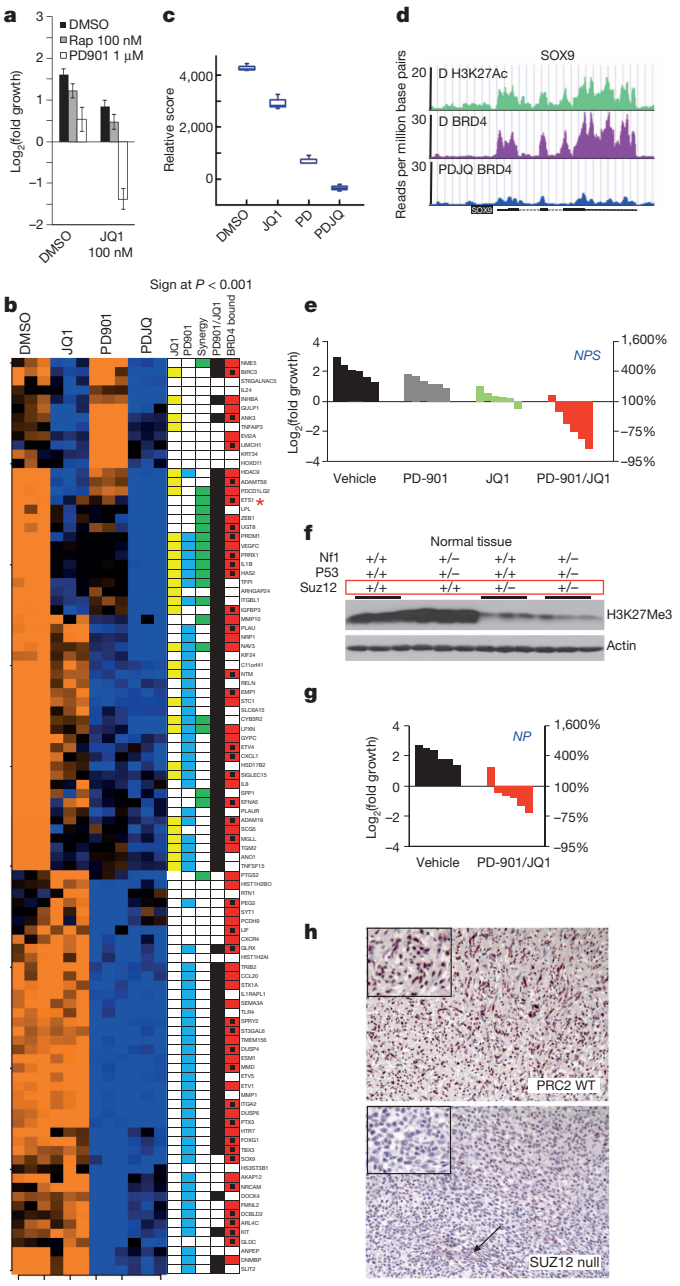

Figure 4 | JQ1 and MEK inhibitors cooperate to promote cell death, suppress Ras transcriptional output and promote tumour regression. **a**, Log_2 of fold change in MPNST cell number (90-8TL). Only cells treated with PD-901 and JQ1 die. Error bars, s.d. ($n = 3$, biological replicate). **b**, Heat map of microarray expression data evaluating the effects of the indicated drugs in *SUZ12/NF1* null cell line 90-8TL (Ras signature gene set: see Supplementary Table 2). Genes significantly ($P < 0.001$) downregulated are indicated (JQ1, yellow; PD901, blue; PD901/JQ1, black). Genes uniquely or more potently suppressed by PD901/JQ1 are indicated in green. BRD4-bound genes are indicated in red. H3K27Ac and BRD4 were significantly enriched at the promoters of downregulated genes (compared with overall genes bound; 72% versus 46%, Fisher's exact test, $P = 7.9 \times 10^{-3}$). A red box with black square denotes a minimum fourfold displacement of BRD4 in response to PD901/JQ1. H3K27Ac and BRD4 binding overlaps at 69/71 promoters. **c**, Box plot of ssGSEA comparing the enrichment of our Ras signature gene set after treatments. The output shows cooperativity of JQ1 and PD901 in suppressing this Ras signature ($n = 3$, biological replicate). **d**, Gene tracks of H3K27Ac and BRD4 ChIP-seq occupancy at SOX9 after DMSO or PD901/JQ1 treatment (*y* axis, reads per million base pairs). **e**, Waterfall plot of MPNSTs from *Nf1/p53/Suz12* mice treated with vehicle control, PD-0325901, JQ1 or a combination of PD-0325901 and JQ1 (10 days). **f**, Immunoblots of H3K27me3 in lung tissue of WT, *Nf1/p53*, $SUZ12^{+/-}$ and *Nf1/p53/Suz12* mice. H3K27Me3 levels are disproportionately low in all animals carrying one mutant *SUZ12* allele. **g**, Waterfall plot of MPNSTs from *Nf1/p53* mice comparing vehicle with combination of PD-0325901 and JQ1 ($P = 5.4 \times 10^{-4}$, *t*-test). **h**, Immunohistochemistry comparing H3K27me3 expression in a human MPNST that is WT for PRC2 genes (P6) and a SUZ12 null tumour (P7). Arrow depicts positive staining of blood vessel. An additional tumour set is shown in Extended Data Fig. 4d, and results from all primary MPNSTs that were evaluated are shown in Extended Data Table 1.

Extended Data Table 1). Together, these studies reveal a promising therapeutic strategy for MPNSTs, and suggest that PRC2 genetic alterations or H3K27me3/H3K27Ac levels could be used as biomarkers for selection of patients.

While the PRC2 complex is oncogenic in many cancers, these studies reveal an important tumour-suppressive function for two PRC2 components in *NF1*-deficient solid tumours. Moreover, this complex appears to function as a rheostat for Ras-dependent transcription. It is becoming apparent that the oncogenic Ras signal is amplified as cancers progress. Because *NF1*-mutant tumours are driven by a relatively weak oncogenic signal and lack an amplifiable mutant *RAS* allele, *SUZ12* loss may be a particularly important mechanism of signal potentiation. PRC2 inactivation may also enhance Ras-driven transcription in *RAS*-mutant cancers. However, further studies will be required to assess this possibility.

Additionally, these studies demonstrate that *SUZ12* loss promotes an epigenetic switch from H3K37Me3 to H3K27Ac, conferring sensitivity to BRD4 inhibitor-based combination therapies. Our data suggest that BRD4 inhibitors alone may not be effective in these tumours, but should be evaluated in combination with MEK inhibitors. However, this work may also have other important clinical implications. EZH2 inhibitors have therapeutic potential in cancers with mutated or overexpressed *EZH2*. Given the prevalence of *SUZ12* and *EED* alterations, it may be prudent to screen for these events in broader clinical trials, as EZH2 inhibitors could exacerbate potential pro-tumorigenic effects of heterozygous alterations. Regardless, these studies reveal a mechanistic link between Ras and PRC2, and provide a scientific rationale for developing a new therapeutic combination for tumours that are currently untreatable.

Online Content Methods, along with any additional Extended Data display items and Source Data, are available in the online version of the paper; references unique to these sections appear only in the online paper.

Received 4 December 2013; accepted 6 June 2014.
Published online 13 August 2014.

1. Sauvageau, M. & Sauvageau, G. Polycomb group proteins: multi-faceted regulators of somatic stem cells and cancer. *Cell Stem Cell* **7,** 299–313 (2010).
2. Ernst, T. *et al.* Inactivating mutations of the histone methyltransferase gene EZH2 in myeloid disorders. *Nature Genet.* **42,** 722–726 (2010).
3. Zhang, J. *et al.* The genetic basis of early T-cell precursor acute lymphoblastic leukaemia. *Nature* **481,** 157–163 (2012).
4. Maertens, O. & Cichowski, K. An expanding role for RAS GTPase activating proteins (RAS GAPs) in cancer. *Adv. Biol. Regul.* **55,** 1–14 (2014).
5. Downward, J. Targeting RAS signalling pathways in cancer therapy. *Nature Rev. Cancer* **3,** 11–22 (2003).
6. Shaw, A. T. *et al.* Sprouty-2 regulates oncogenic K-ras in lung development and tumorigenesis. *Genes Dev.* **21,** 694–707 (2007).
7. Feldser, D. M. *et al.* Stage-specific sensitivity to p53 restoration during lung cancer progression. *Nature* **468,** 572–575 (2010).
8. Junttila, M. R. *et al.* Selective activation of p53-mediated tumour suppression in high-grade tumours. *Nature* **468,** 567–571 (2010).
9. Xu, J. *et al.* Dominant role of oncogene dosage and absence of tumor suppressor activity in Nras-driven hematopoietic transformation. *Cancer Discov.* **3,** 993–1001 (2013).
10. McLaughlin, S. K. *et al.* The RasGAP gene, *RASAL2*, is a tumor and metastasis suppressor. *Cancer Cell* **24,** 365–378 (2013).
11. Min, J. *et al.* An oncogene-tumor suppressor cascade drives metastatic prostate cancer by coordinately activating Ras and nuclear factor-κB. *Nature Med.* **16,** 286–294 (2010).
12. De Raedt, T. *et al.* Genomic organization and evolution of the NF1 microdeletion region. *Genomics* **84,** 346–360 (2004).
13. Lopez-Correa, C. *et al.* Recombination hotspot in NF1 microdeletion patients. *Hum. Mol. Genet.* **10,** 1387–1392 (2001).

14. De Raedt, T. *et al.* Elevated risk for MPNST in NF1 microdeletion patients. *Am. J. Hum. Genet.* **72,** 1288–1292 (2003).
15. Mautner, V. F. *et al.* Clinical characterisation of 29 neurofibromatosis type-1 patients with molecularly ascertained 1.4 Mb type-1 NF1 deletions. *J. Med. Genet.* **47,** 623–630 (2010).
16. Beroukhim, R. *et al.* Assessing the significance of chromosomal aberrations in cancer: methodology and application to glioma. *Proc Natl Acad Sci USA* **104,** 20007–20012 (2007).
17. McGillicuddy, L. T. *et al.* Proteasomal and genetic inactivation of the NF1 tumor suppressor in gliomagenesis. *Cancer Cell* **16,** 44–54 (2009).
18. Cichowski, K. *et al.* Mouse models of tumor development in neurofibromatosis type 1. *Science* **286,** 2172–2176 (1999).
19. Legius, E. *et al.* TP53 mutations are frequent in malignant NF1 tumors. *Genes Chromosom. Cancer* **10,** 250–255 (1994).
20. Beert, E. *et al.* Atypical neurofibromas in neurofibromatosis type 1 are premalignant tumors. *Genes Chromosom. Cancer* **50,** 1021–1032 (2011).
21. Pasini, D. *et al.* Characterization of an antagonistic switch between histone H3 lysine 27 methylation and acetylation in the transcriptional regulation of Polycomb group target genes. *Nucleic Acids Res.* **38,** 4958–4969 (2010).
22. Filippakopoulos, P. *et al.* Histone recognition and large-scale structural analysis of the human bromodomain family. *Cell* **149,** 214–231 (2012).
23. Filippakopoulos, P. *et al.* Selective inhibition of BET bromodomains. *Nature* **468,** 1067–1073 (2010).
24. Widemann, B. C. Current status of sporadic and neurofibromatosis type 1-associated malignant peripheral nerve sheath tumors. *Curr. Oncol. Rep.* **11,** 322–328 (2009).
25. Delmore, J. E. *et al.* BET bromodomain inhibition as a therapeutic strategy to target c-Myc. *Cell* **146,** 904–917 (2011).
26. Puissant, A. *et al.* Targeting MYCN in neuroblastoma by BET bromodomain inhibition. *Cancer Discov.* **3,** 308–323 (2013).
27. Johannessen, C. M. *et al.* TORC1 is essential for NF1-associated malignancies. *Curr. Biol.* **18,** 56–62 (2008).
28. De Raedt, T. *et al.* Exploiting cancer cell vulnerabilities to develop a combination therapy for ras-driven tumors. *Cancer Cell* **20,** 400–413 (2011).
29. Chang, T. *et al.* Sustained MEK inhibition abrogates myeloproliferative disease in Nf1 mutant mice. *J. Clin. Invest.* **123,** 335–339 (2013).
30. Jessen, W. J. *et al.* MEK inhibition exhibits efficacy in human and mouse neurofibromatosis tumors. *J. Clin. Invest.* **123,** 340–347 (2013).

Supplementary Information is available in the online version of the paper.

Acknowledgements This work was supported by the following organizations: The US Department of Defense (W81XWH-11-1-0138), the Ludwig Center at DF/HCC and the Children's Tumor Foundation (K.C.); T.D. was a recipient of the Young Investigator Award of the Children's Tumor Foundation; FWO-Flanders G.0784.10N (E.L.). E.B. was a recipient of an Emmanuel Vanderschueren Fellowship from the Vlaamse Liga tegen Kanker. Association Neurofibromatoses et Recklinghausen, Ligue Française Contre les Neurofibromatoses, Association pour la Recherche sur le Cancer, Comité de Paris de la Ligue Contre le Cancer, the French Clinical Research program (PHRC 2002, P. Wolkenstein) and INSERM (Nf1GeneModif project) (M.V. and E.P.). We thank the Platform of Biological Resources, Assistance Publique Hôpitaux de Paris, Hôpital Henri Mondor, Créteil, France, for providing tissue samples.

Author Contributions T.D. and K.C. conceived and designed the functional studies and mouse experiments. E.L. E.B., M.V., E.P. and A.L. conceived, designed and performed the genomic studies. T.D. performed the cellular, mouse, microarray and ChiP-seq experiements. H.B. coordinated human sample acquisition and analysis. E.L., M.U., V.M., H.K. and M.V. provided human MPNST samples. N.O. performed immunohistological staining. K.H. provided the SUZ12 mice and advice. J.L.H. performed pathological analysis. W.C. assisted in evaluating mouse neurofibromas. J.B. provided compounds and advice. T.D. and K.C. wrote the manuscript. All authors discussed the results and commented on the manuscript.

Author Information All microarray data have been deposited in the Gene Expression Omnibus database under accession number GSE52777. Reprints and permissions information is available at www.nature.com/reprints. The authors declare no competing financial interests. Readers are welcome to comment on the online version of the paper. Correspondence and requests for materials should be addressed to K.C. (kcichowski@rics.bwh.harvard.edu) or E.L. (Eric.Legius@uzleuven.be).

METHODS

Human MPNST samples. All patients were diagnosed as having neurofibromatosis type I. Consent was obtained for tissue acquisition according to Institutional review board approved protocol and local ethical committees.

Cell lines and reagents. ST88-14 (J. Fletcher), 90-8TL (E. Legius), S462 (E. Legius), SNF96.2 (ATCC), U251 (ATCC), A172 (ATCC), T98G (ATCC), MEWO (ATCC), WM3526, Colo-741, RKO (ATCC), H460 (ATCC) and H1355 (ATCC) are human MPNST, GBM, melanoma, colon and lung cancer cell lines. 702T is a mouse *Nf1/p53/Suz12*-deficient MPNST cell line. All cell lines were tested and negative for mycoplasma. Antibodies were obtained from the following sources: H3K27Me3 (9733), H3K27Ac (4353), pERK (XP, 4370) and Vinculin (4670) (Cell Signaling Technologies); SUZ12 (sc-46264) (Santa Cruz Biotechnology); actin (A2066) (Sigma). For ChIP-seq, the following antibodies were used: BRD4 (Bethyl, A301-085A) and H3K27Ac (Abcam ab4729).

Cell counting, IC_{50} and proliferation curves. All counting experiments were done by haemocytometer. Cells were plated in triplicate for each condition (treatment or genetic alteration). The following day the exact number of cells plated was determined (day 0 value) and cells were treated with conditioned media. The number of cells was determined after 3 (normal growth conditions) or 6 (limiting growth factors) days or precisely after three population doublings to determine values of IC_{50}. Fold growth or $\log_2$ of fold of the number of cells was determined versus day 0. When cell death was induced (compared with the number of cells plated on day 0), data were plotted as $\log_2$ of fold cell number (negative values indicate cell death). IC_{50} values and 95% confidence intervals were determined using GraphPad Prism 5 software.

Array comparative genomic hybridization. Array comparative genomic hybridization experiments (Agilent 244K and 400K) were performed as previously described[20]. Array comparative genomic hybridization data (Agilent 244K) from 21 independent, high-grade MPNSTs (HM1, 2, 3, 5–8, 10, 12, 13, 15, 17, 19, 20, 22–26, 28, and 30) were used as published previously[20]. Digestion, labelling and hybridization of tumour- and patient- or gender-matched blood DNA were performed according to the manufacturer's instructions (Agilent).

Sequencing. The coding sequences of 14 H3K27me3-related genes were analysed (*AEBP2*, *EED*, *EZH2*, *EZH1*, *HDAC2*, *JARID2*, *PCL1*, *PCL2*, *PCL3*, *RBBP4*, *RBBP7*, *SIRT1*, *SUZ12* and *UTX*) using a targeted next generation sequencing (NGS) approach. Experiments were performed on the NGS platform of the Cochin Hospital, Paris (Assistance Publique, Hôpitaux de Paris, France). Briefly, the custom primers panel targeting the 14 genes (coding exons and IVS boundaries) was designed using the AmpliSeq Designer (Life Technologies). NGS library preparation used the Ion AmpliSeq Library Kit 2.0 according to the manufacturer's instructions (Ion AmpliSeq Library Preparation, publication part number MAN0006735, revision 5.0, July 2013, Life Technologies). Amplified libraries were purified using Agencourt AMPure XP beads (Beckman Coulter). Prior to library pooling and sequencing sample preparation, amplified libraries were validated and quantified using the 2100 Bioanalyzer microfluidic platform (Agilent Technologies). Emulsion PCR used the Ion OneTouch Instrument. Enrichment of the template-positive Ion OneTouch 200 ion sphere particle PCR used the Ion OneTouch ES (Life Technologies). The template-positive ion sphere particles were loaded on Ion 318 chips and sequenced with an Ion PGM sequencer (Life Technologies). Sequence alignment and extraction of single nucleotide polymorphisms and short insertions/deletions were performed using the Variant Caller plugin on the Ion Torrent Browser, and DNA sequences visualized using the Integrated Genomics Viewer (version 2.3) from the Broad Institute. NextGENe software (version 2.3.3, Softgenetics), was also used for sequence alignment, extraction of single nucleotide polymorphisms and short indels, and their visualization.

Real-time PCR. Cell were scraped and dissolved in Trizol reagent (Invitrogen). RNA was treated with DNaseI (Roche) and reverse transcribed using the qScript Reverse transcriptase kit (Quanta). Real-time PCR analysis used the PerfeCTa SYBR Green kit (Quanta) for *BRD4* (5′-CATGGACATGAGCACAATCA-3′ 5′-TCATGGTCAGGAGGGTTGTA-3′).

RNA interference and complementary DNA expression. Non-targeting short interfering RNAs (siRNAs) (D-001810-10: 5′-UGGUUUACAUGUCGACUAA-3′; 5′-UGGUUUACAUGUUGUGUGA-3′; 5′-UGGUUUACAUGUUUUCUGA-3′; 5′-UGGUUUACAUGUUUUCCUA-3′) and siRNAs against BRD4 (ON-TARGET smartpool siRNA L-004937-00: 5′-UGGUUUACAUGUCGACUAA-3′; 5′-UGGUUUACAUGUUGUGUGA-3′; 5′-UGGUUUACAUGUUUUCUGA-3′; 5′-UGGUUUACAUGUUUUCCUA-3′) were purchased from Dharmacon. siRNAs were transfected with lipofectamine RNAiMAX from Invitrogen. Lentiviral pLKO vectors were obtained from the RNAi consortium of the Broad Institute. shSUZ12 S1 (NM_015355.1-2076s1c1, target sequence 5′- GCTGACAATCAAATGAATCAT-3′), shSUZ12 S2 (NM_015355.1-668s1c1, target sequence 5′GCTTACGTTTACTGGTTTCTT-3′) and shSUZ12 S3 (NM_015355.1-501s1c1, target sequence 5′-CGGAATCTCATAGC ACCAATA-3′) were used to target SUZ12. Human *SUZ12* (Open Biosystems) was cloned into a pLenti CMV/TO Puro vector. Lentiviral infections were performed as previously described[28].

Expression micro-array and gene set enrichment analysis. The MPNST cell line 90-8TL was infected with LACZ control or SUZ12 and cultured for 14 days. The LACZ expressing 90-8TL cell line was also treated with 100 nM JQ1, PD0325901 2 μM, a combination of PD0325901 (2 μM) and JQ1 (100 nM) or vehicle (DMSO) for 24 h. Additionally SUZ12 was knocked down in the U251 cell line by shRNA. All experiments were performed in triplicate. RNA was extracted using Trizol reagent (Invitrogen) and purified using Qiagen RNeasy extraction kit (according to the manufacturer's instructions) and hybridized to the Affymetrix Human Gene 1.0 ST array by the Partners HealthCare Center for Personalized Genetic Medicine core. Analyses used BRB-ArrayTools developed by R. Simon and the BRB-ArrayTools development team. Thresholds were set at $P < 0.001$. Supplementary Table 3 lists all the genes significantly changed ($P < 0.001$) compared with control. We first made a *SUZ12* gene list of genes that were downregulated at least twofold ($P < 0.001$) in *SUZ12* reconstituted cells (Supplementary Table 1). GSEA[31] and ssGSEA used the Broad Institute interface (www.broadinstitute.com/gsea/index.jsp). Several gene lists upregulated by Ras activation were significantly enriched in our experiments (BILD_HRAS_ONCOGENIC_SIGNATURE, KRAS.300_UP.V1_UP, KRAS.600_UP.V1_UP, KRAS.600.LUNG.BREAST_UP.V1_UP, KRAS.BREAST_UP.V1_UP). To identify more specifically a subset of direct suppressive effects on the Ras pathway, we first compiled these five significant gene lists and selected those genes that were significantly repressed by JQ1, PD-901 or combined JQ1/PD901 in MPNSTs (Supplementary Table 2) (class comparison of all treatments at $P < 0.001$).

ChIP-seq analysis. BRD4, H3K27Me3 and H3K27Ac were ChIPed following the Agilent Mammalian ChIP-on-chip protocol. 90-8TL cells were grown and treated under the same conditions as performed for microarray studies. Cells were cross-linked for 15 min at room temperature by the addition of one-tenth of the volume of 11% formaldehyde solution to the growth media. Pull down was performed with the indicated antibodies and DNA was submitted for sequencing to the CCCB core of the Dana-Farber Cancer Institute.

Alignment used the BWA package. Mapped tags were analysed using a statistical method that fitted a Poisson distribution to the data and calculated a global false discovery rate for peak detection. Peak calling used the HOMER software package with the false discovery rate set to 0.001. Peak calling in this setting is differential because the algorithm requires that the number of tags mapped to an identified peak region is fourfold higher in the test sample than the input sample. A background filter was applied by analysing a 10 kilobase region surrounding each peak. Peaks were removed unless tag density within each peak was at least fourfold higher than in the surrounding region. Peaks were only called in regions of the genome that were not masked by standard repeat element filters. Although repeat areas were removed, some regions of the genome still had low mapability due to undetected repeats or genome duplications. Accordingly, a final filter removed peaks in such poorly mappable regions. Differential peaks (comparing binding in different treatment groups) were also determined by the HOMER package.

Mouse models and pathology. Animal procedures were approved by the Center for Animal and Comparative Medicine in Harvard Medical School in accordance with the National Institutes of Health Guide for the Care and Use of Laboratory Animals and the Animal Welfare Act. c57bl/6 $Nf1^{+/-}$ (ref. 32) and $Suz12^{+/-}$ (ref. 33) were crossed to generate double heterozygous mice. These mice were intercrossed further to generate $Nf1^{+/-}; Suz12^{+/-}$ mice with both genes in a *cis* configuration. Similarly $Nf1^{+/-}; Suz12^{+/-}$ mice were crossed to $p53^{+/-}$ mice to generate NPS mice having *Nf1*, *Suz12* and *p53* mutations in *cis* on chromosome 11. For our survival studies we used 15 animals in control groups and 30 animals in test groups. Relevant tumour types were evaluated by a human pathologist (J.H.). The pathologist was blinded to the group allocation.

Malignant peripheral nerve sheath tumour. The tumours are composed of fascicles of spindle cells with elongated, wavy nuclei, coarse chromatin and pale, eosinophilic cytoplasm. Scattered tumour cells show marked pleomorphism, including multinucleated forms. There are frequent mitotic figures.

High-grade glioma. The brain is infiltrated by a markedly hypercellular tumour composed of rounded cells with hyperchromatic to vesicular nuclei and variably prominent nucleoli, including occasional large and multinucleated cells.

Olfactory neuroblastoma. Tumours are composed of primitive polygonal cells with vesicular chromatin, prominent, often multiple nucleoli, amphophilic cytoplasm and frequent mitotic figures. The tumour cells are arranged in sheets and form numerous rosettes, and there is multifocal necrosis.

Melanocytic nevus. Heavily black-pigmented lesion (consistent with melanin). The lesional cells are uniform with small nuclei and no nuclear atypia or mitotic activity. The lesion is well circumscribed and does not infiltrate into adjacent tissues.

Intestinal adenoma. These dysplastic polyps (adenomas) show a tubular architecture and are composed of columnar cells with enlarged and elongated, hyperchromatic nuclei with prominent nucleoli and increased mitotic activity.

Drug treatment, dosing schedule and tumour volume measurements. Only mice that developed an MPNST that was readily measurable by Vernier callipers were included in the study. As these tumours develop spontaneously over time, and to ensure adequate randomization, mice were sequentially enrolled per treatment arm, starting with the combination treatment arm. The investigator was not blinded. To have sufficient power (80%) to detect a minimum of 50% tumour shrinkage versus day 0 ($P = 0.05$), we enrolled six animals per treatment group. Mice were enrolled in the study when tumour size reached 300–700 mm^3. Tumour size was measured every 2–3 days by Vernier callipers. Tumour volume was calculated using the standard formula $L \times W^2 \times 52$. Tumour volume and $\log_2$ of fold growth versus day 0 were calculated and plotted on a graph. JQ1 (45 mg/kg) was administered intraperitoneally daily in a 10% (2-hydroxypropyl)-β-cyclodextrin solution (C0926, Sigma). PD-0325901 was administered by oral gavage daily at 1.5 mg/kg (vehicle (0.5% (w/v) methylcellulose solution with 0.2% (v/v) polysorbate 80 (Tween 80)). Compounds given in combination were administered sequentially.

Statistics. Unless otherwise stated, all statistical analysis used SYSTAT 12 software. For each data set, basic statistical values (mean and s.d.) were calculated and normality determined (Shapiro–Wilk normality test); all data sets were normally distributed. All fold change tumour volumes for the different drug combinations were compared by Student's *t*-test (unequal variance). Survival analysis used the Mantel–Cox test. The statistical tests used are mentioned throughout the text.

31. Subramanian, A. *et al.* Gene set enrichment analysis: a knowledge-based approach for interpreting genome-wide expression profiles. *Proc. Natl Acad. Sci. USA* **102,** 15545–15550 (2005).
32. Jacks, T. *et al.* Tumour predisposition in mice heterozygous for a targeted mutation in Nf1. *Nature Genet.* **7,** 353–361 (1994).
33. Pasini, D., Bracken, A. P., Jensen, M. R., Lazzerini Denchi, E. & Helin, K. Suz12 is essential for mouse development and for EZH2 histone methyltransferase activity. *EMBO J.* **23,** 4061–4071 (2004).

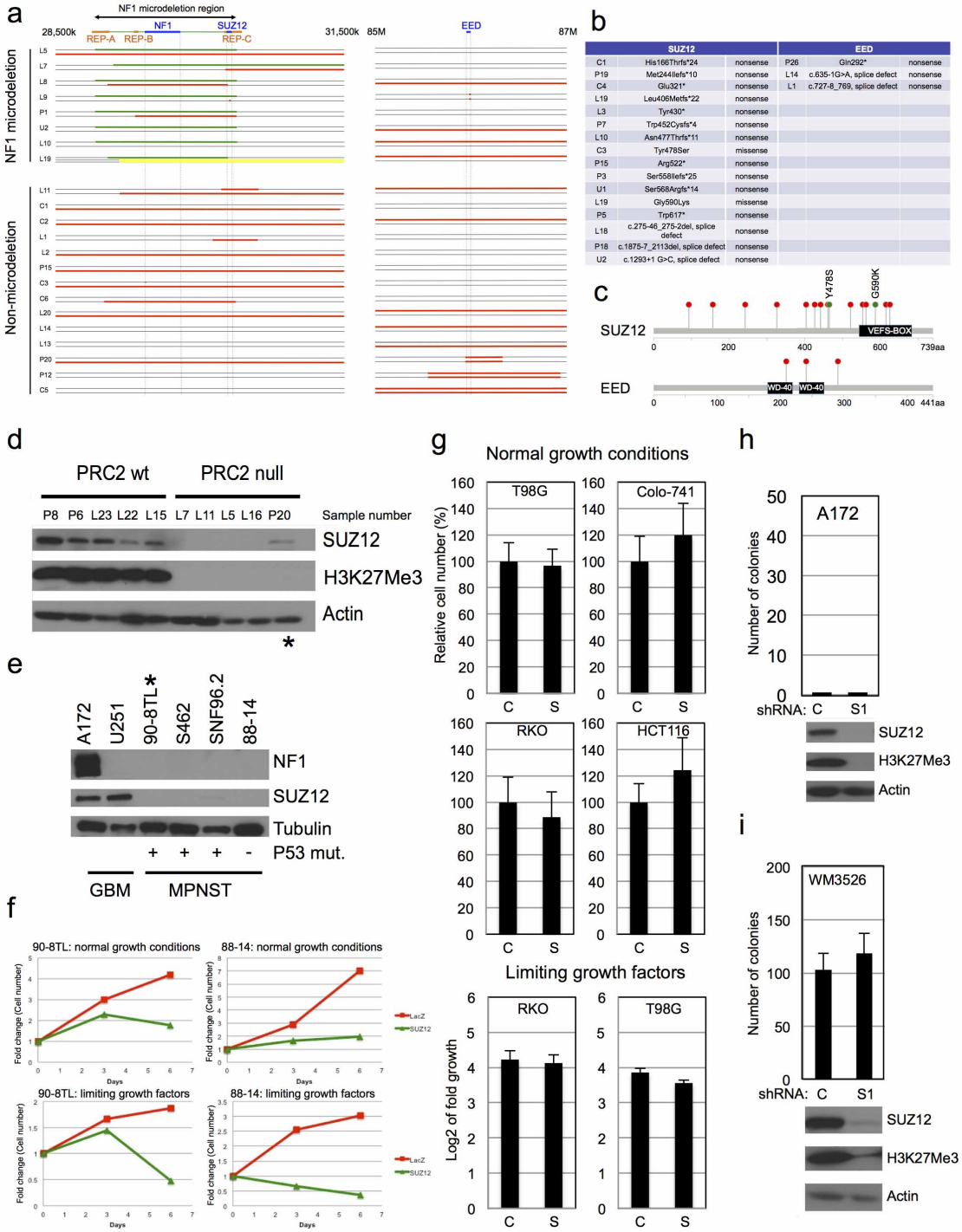

Extended Data Figure 1 | Mutational data in human MPNSTs and further biological analysis of SUZ12 loss. **a**, Schematic overview of the deletions in the *NF1*, *SUZ12* and *EED* regions observed in human MPNSTs (green, germline deletion; red, somatic deletion; yellow, duplication). **b**, List of the amino-acid changes or deletions found in SUZ12 and EED in human MPNSTs. **c**, Schematic representation of the location of *SUZ12* and *EED* mutations (red, truncating mutation; green, missense mutation with amino-acid change noted). **d**, Immunoblots of lysates from primary human MPNSTs. Tumours with homozygous inactivating mutations in one of the PRC2 components (*SUZ12* or *EED*) show complete loss of H3K27Me3. *Homozygous inactivation of EED. **e**, Immunoblots comparing NF1, SUZ12 and H3K27me3 expression of four human MPNST cell lines. *Cell line derived from an MPNST of a patient with an NF1 microdeletion. The human GBM cell lines A172 and U251 were used as a control. Corresponding *NF1* mutations are reported in Extended Data Table 1 (S462, L2; 90-8TL, L3) and elsewhere in these *NF1*-deficient lines. p53 mutations, when known, are denoted and reported elsewhere[20]. **f**, Proliferation curves used to derive bar graphs shown in Fig. 1d (red, LacZ control; green, SUZ12 reconstituted). **g**, Relative proliferation of several SUZ12 WT cell lines: colon (RKO, colo741, HCT-116) or GBM (T98G), after introduction of a control or SUZ12 lentivirus. None of these cell lines exhibited a significant decrease in proliferation under normal growth conditions or cell death in limiting growth factors, in contrast to SUZ12-deficient cells shown in Fig. 1d. **h**, Effects of shSUZ12 (S1) on colony formation (top) and SUZ12 expression (bottom) in A172 GBM cells, which are *NF1* WT (see Extended Data Fig. 1e). **i**, Effects of shSUZ12 (S1) on SUZ12 expression and colony formation in WM3526 melanoma cells, which are *NF1* WT. Error bars, s.d. ($n = 3$, biological replicates).

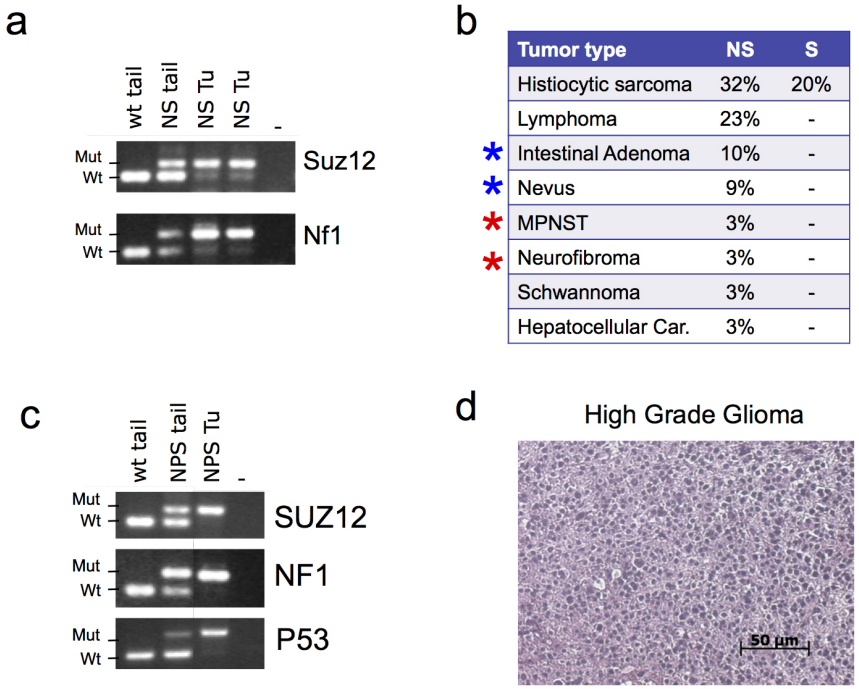

	Tumor type	NS	S
	Histiocytic sarcoma	32%	20%
	Lymphoma	23%	-
*	Intestinal Adenoma	10%	-
*	Nevus	9%	-
*	MPNST	3%	-
*	Neurofibroma	3%	-
	Schwannoma	3%	-
	Hepatocellular Car.	3%	-

Extended Data Figure 2 | *Suz12* and *Nf1* mutations cooperate to promote widespread tumour development in mice. **a**, Semi-quantitative PCR showing loss of the WT *Suz12* and *Nf1* allele in *Nf1*/*Suz12* mouse tumours. **b**, Table listing the tumours observed in $Nf1^{+/-}$; $Suz12^{+/-}$ and $Suz12^{+/-}$ mice. Tumour types denoted with a red asterisk occur in patients with NF1 and an increased frequency in patients with NF1 microdeletions. Tumour types denoted with a blue asterisk represent spontaneous tumour types/lesions that have been shown to harbour NF1 mutations humans. **c**, Semi-quantitative PCR showing loss of the WT *Suz12*, *Nf1* and *p53* allele in *Nf1*/*p53*/*Suz12* mouse MPNST. **d**, Haematoxylin and eosin staining of a GBM from an *Nf1*/*p53*/*Suz12* mouse.

a

	SUZ12			JQ1		
	NES	p-value	FDR	NES	p-value	FDR
KONDO_EZH2_TARGETS	1.65	1.95 10^{-3}	0.07	2.00	0	0.00
BILD_HRAS_ONCOGENIC_SIGNATURE	1.52	0	0.12	1.68	0	0.04
KRAS.300_UP.V1_UP	1.48	9.96 10^{-3}	0.15	1.53	4.53 10^{-3}	0.09
KRAS.600_UP.V1_UP	1.75	0	0.05	1.34	2.34 10^{-2}	0.21
KRAS.600.LUNG.BREAST_UP.V1_UP	1.46	1.89 10^{-3}	0.16	1.69	0	0.04
KRAS.BREAST_UP.V1_UP	1.45	1.83 10^{-2}	0.16	1.78	00	0.02

b

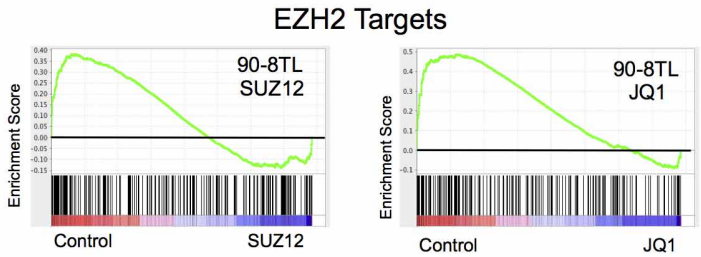

c

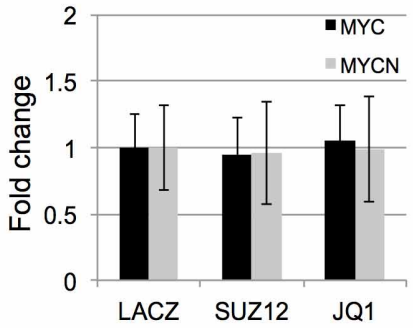

d

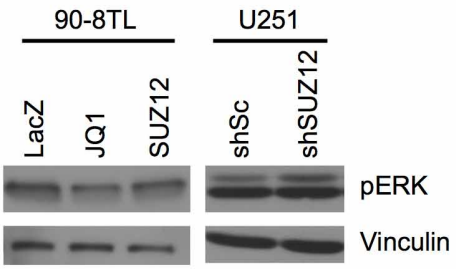

Extended Data Figure 3 | Microarray data analysis (GSEA) and pERK levels in response to *SUZ12* modulation and JQ1 treatment. **a**, Table showing that PRC2 (EZH2) and Ras signatures were suppressed in MPNST cells reconstituted with SUZ12 or treated with JQ1. Also shown are normalized enrichment score, *P* value and false discovery rate. **b**, EZH2 signature enrichment plots (using the KONDO_EZH2 data set obtained from the Molecular Signatures Database) in MPNSTs reconstituted with SUZ12, versus vector control, or treated with JQ1, versus vehicle control (100 nM, 24 h, triplicate samples). Plots show a significant downregulation of the EZH2 signature after SUZ12 reconstitution and JQ1 treatment. **c**, Microarray expression analysis in human MPNST cells shows that expression of MYC and MYCN is unaltered after SUZ12 reconstitution or treatment with JQ1. Error bars, s.d. ($n = 3$, biological replicates). **d**, Phospho-ERK levels did not appreciably change in response to *SUZ12* loss (U251), reconstitution (90-8TL) or JQ1 treatment (90-8TL).

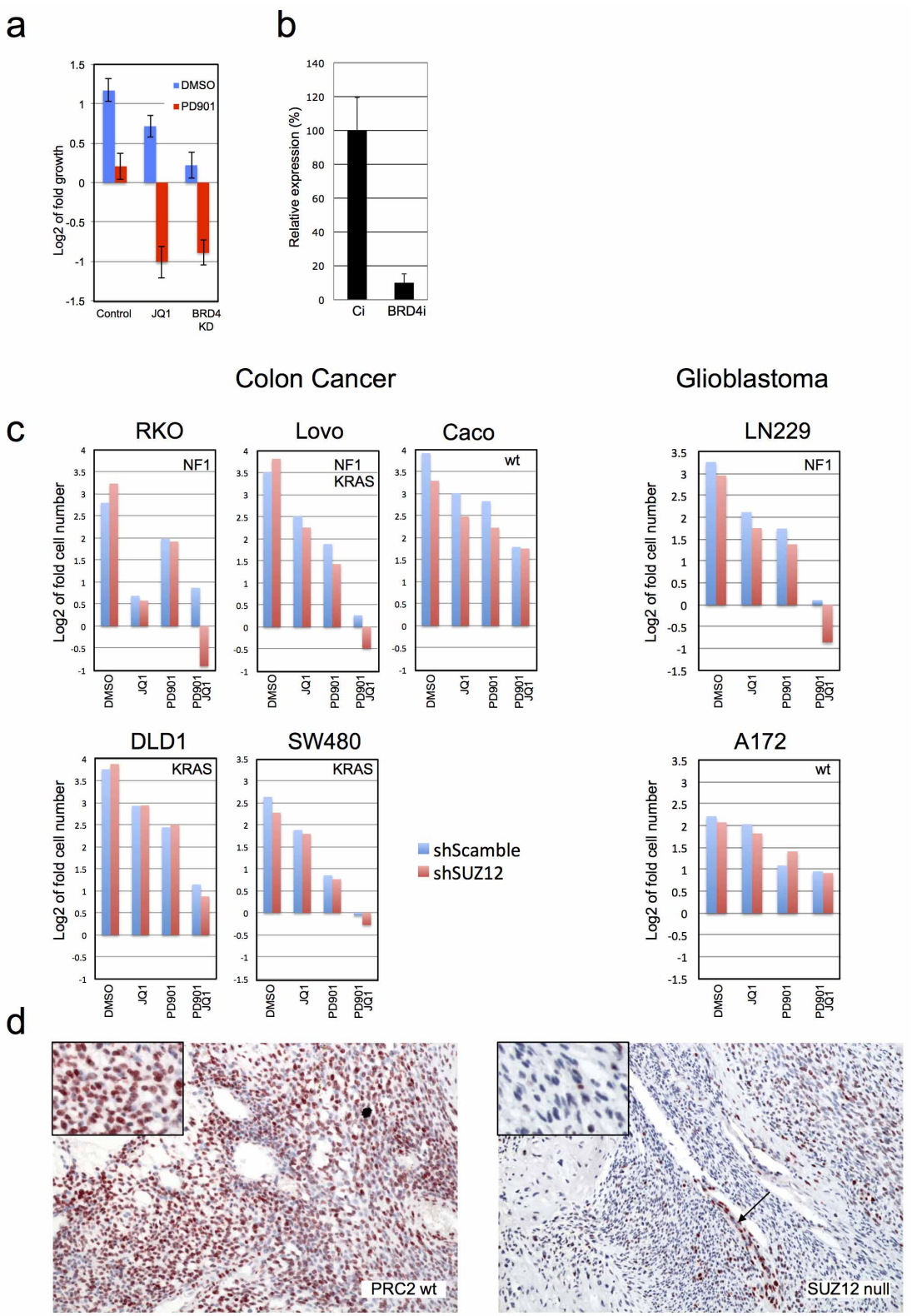

Extended Data Figure 4 | Consequences of SUZ12 loss on drug sensitivity and H3K27me3 levels. **a**, Graph depicting $\log_2$ fold change in MPNST cell number (90-8TL) after 3 days in response to drugs and siRNA sequences indicated. PD-0325901 also cooperates with genetic BRD4 ablation to kill cells. **b**, Relative expression of BRD4 as determined by real-time PCR after exposure to BRD4-specific siRNAs (90-8TL). **c**, *SUZ12* ablation using shSUZ12 S1 conferred increased sensitivity to combined PD-901/JQ1 in *NF1*-deficient but not NF1 WT colon cancer and GBM cell lines. Log_2 fold change in cell number was determined. RKO, DLD1 and Caco cell lines were treated with 1 μM JQ1 and 1 μM PD901 each time alone or in combination. The Lovo cell line was treated with 500 nM JQ1 and 250 M PD901; SW480 was treated with 250 nM PD901 and 1 μM JQ1; LN229 and A172 cell lines were treated with 500 nM JQ1 and 1 μM PD901. **d**, Immunohistochemistry comparing H3K27me3 expression in an additional human MPNST that was WT for *SUZ12* and other PRC2 genes, and one that was null for *SUZ12*. Arrow depicts positive staining of blood vessel. Staining of additional tumours is shown in Extended Data Table 1. Error bars, s.d. ($n = 3$, biological replicates).

Extended Data Table 1 | Combined deletion and mutational data for tumours listed in Fig. 1

	SAMPLE	NF1		SUZ12		EED		H3K27Me3 IHC
		germline	somatic	first hit	second hit	somatic 1	somatic 2	
NF1 MICRODELETION	L10(HM12)	type 1 MD	not deleted, mutation NE	germline type 1 MD	somatic c.1430del; p.(Asn477Thrfs*11)	chr11:hg19:g[62,371,499_62,341,498]_[134,927,055_134,927,114]del	-	NE
	L16 (HM20)	type 1 MD	not deleted, mutation NE	germline type 1 MD	somatic c.1768G>A; p.(Gly590Lys)	-	-	NE
	L19 (HM24)	type 2 MD	chr17:hg19:g[29,169_29,228]_[81,124,168_81,124,227]dup	germline type 2 MD	somatic chr17:hg19:g[29,169_29,228]_[81,124,168_81,124,227]dup; somatic c.1716_1719delinsATGA, p.(Leu406Metfs*22)	chr11:hg19:g[192,372_192,431]_[134,927,055_134,927,114]del	-	Positive
	L3 (HM3) = 90-BTL	type 1 MD	not deleted, mutation NE	germline type 1 MD	somatic c.1290T>A; p.(Tyr430*)	-	-	NE
	L5 (HM5)	type 1 MD	chr17:hg19:g[25,318,639_25,318,698]_[34,462,427_34,462,486]del	germline type 1 MD	somatic chr17:hg19:g[25,318,639_25,318,698]_[34,462,427_34,462,486]del	-	-	NE
	L7 (HM7)	chr17:hg19:g[28,999,834_28,999,893]_[33,898,314_33,898,373]del	chr17:hg19:g[30,262,897_30,262,986]_[30,333,079_30,333,138]del	germline chr17:hg19:g[28,999,834_28,999,893]_[33,898,314_33,898,373]del	somatic chr17:hg19:g[30,262,897_30,262,986]_[30,333,079_30,333,138]del	-	-	pLoss
	L8 (HM8)	type 1 MD	type 2 MD	germline type 1 MD	somatic type 2 MD	chr11:hg19:g[192,372_192,431]_[134,927,055_134,927,114]del	-	Loss
	L9 (HM10)	type 1 MD	not deleted, mutation NE	germline type 1 MD	somatic AMPL:S30772616 chr17:hg19:g[30,302,416_30,302,593]del; AMPL:S30798640 chr17:hg19:g[30,302,585_30,302,756]del	chr11:hg19:g[85,988,023_85,988,082]_[85,988,016_85,988,075]del	chr11:hg19:g[85,988,023_85,988,082]_[85,988,016_85,988,075]del	Loss
	P1	type 1 MD	type 3 MD	germline type 1 MD	somatic type 3 MD	-	-	Loss
	P10	chr17:hg19:g[2,537,850_2,542,770]_[44,351,152_44,787,180]del	c.6799C>T; p.(Gln2267*)	germline chr17:hg19:g[2,537,850_2,542,770]_[44,351,152_44,787,180]del	-	-	-	Loss
	P11	chr17:hg19:g[7_47,546]_[31,644,573_31,647,854]del	c.499_502del; p.(Lys5Glnfs*10)	germline chr17:hg19:g[7_47,546]_[31,644,573_31,647,854]del	-	-	-	NE
	P16	chr17:hg19:g[28,851,905_28,858,444]_[30,451,370_30,458,859]del	c.715C>T; p.(Gln239*)	germline chr17:hg19:g[28,851,905_28,858,444]_[30,451,370_30,458,859]del	-	-	-	NE
	P18	type 1 MD	c.2446C>T; p.Arg816*	germline type 1 MD	somatic c.1875-7_2115del; splice defect	-	-	NE
	P2	chr17:hg19:g[7_47,546]_[43,518,341_43,651,877]del	c.4772+1G>A; splice defect	germline chr17:hg19:g[7_47,546]_[43,518,341_43,651,877]del	-	-	-	NE
	P26	chr17:hg19:g[29,098,392_29,109,733]_[30,289,970_30,293,185]del	c.4103T>A; p.Leu1368*	germline chr17:hg19:g[29,098,392_29,109,733]_[30,289,970_30,293,185]del	-	c.874C>T; p.(Gln292*)	c.874C>T; p.(Gln292*)	NE
	P5	chr17:hg19:g[29,361,835_29,375,967]_[30,604,835_30,610,001]del	c.2903T>G; p.(Met968Arg)	germline chr17:hg19:g[29,361,835_29,375,967]_[30,604,835_30,610,001]del	somatic c.1851G>A; p.(Trp617*)	-	-	NE
	P7	type 2 MD	c.1381C>T; p.Arg461*	germline type 2 MD	somatic c.1356del; p.(Trp452Cysfs*4)	-	-	Loss
	U1	type 1 MD	NE	germline type 1 MD	somatic c.1704del; p.(Ser568Argfs*14)	NE	-	NE
	U2	type 1 MD	NE	germline type 1 MD	somatic c.1293+1G>C; splice defect	chr11:hg19:g[57,409,466_57,609,525]_[119,500,194_119,500,253]del	not deleted, mutation NE	NE
NON MICRODELETION	C1	c.4938insTG; p.(Gly1647Trpfs*31)	chr17:hg19:g[26,734,612_26,734,671]_[30,333,079_30,333,138]del	somatic chr17:hg19:g[26,734,612_26,734,671]_[30,333,079_30,333,138]del	somatic c.490del; p.(His164Thrfs*24)	-	not deleted, mutation NE	NE
	C2	c.2002-14C>G; splice defect	chr17:hg19:g[26,883,246_26,883,301]_[32,578,657_32,578,716]del	somatic chr17:hg19:g[26,883,246_26,883,301]_[32,578,657_32,578,716]del	-	chr11:hg19:g[78,800,489_78,8000,548]_[123,942,399_123,942,458]del	-	NE
	C3	chr17:hg19:g[29,428,900_29,428,959]_[29,483,106_29,483,165]del	chr17:hg19:g[28,121,342_28,121,401]_[34,480,451_34,480,510]del	somatic chr17:hg19:g[28,121,342_28,121,401]_[34,480,451_34,480,510]del	somatic c.1433A>C, p.(Tyr478Ser)	not deleted, mutation NE	not deleted, mutation NE	NE
	C4	c.2705del; p.(Met902Serfs*3)	c.1-?_7394+?del	somatic c.961G>T; p.(Glu321*)	-	NE	NE	NE
	C5	c.1756_1759del; p.Thr586Valfs*18	c.6364+5G>A, splice site	-	-	chr11:hg19:g[84,500,047_84,500,106]_[87,671,742_87,671,801]del	chr11:hg19:g[84,500,047_84,500,106]_[87,671,742_87,671,801]del	NE
	C7	c.3721C>T; p.R1241*	chr17:hg19:g[29,592,992_29,593,051]_[30,244,750_30,244,809]del	-	-	not deleted, mutation NE	not deleted, mutation NE	NE
	C8	c.2041C>T; p.R681*	chr17:hg19:g[29,435,620_29,435,679]_[29,592,992_29,593,051]del	-	-	not deleted, mutation NE	not deleted, mutation NE	NE
	L1 (HM1)	c.4537C>T; p.Arg1513*	not deleted, mutation NE	somatic chr17:hg19:g[30,131,459_30,131,518]_[30,604,685_41,162,744]del	-	c.727-8_769del; splice defect	-	NE
	L11 (HM13)	c.2061C>T; p.Arg681*	chr17:hg19:g[29,169_29,228]_[35,400,357_35,400,416]del	somatic chr17:hg19:g[29,169_29,228]_[35,400,357_35,400,416]del	somatic chr17:hg19:g[30,262,897_30,262,956]_[30,651,201_30,651,260]del	chr11:hg19:g[73,390,675_73,390,734]_[134,927,055_134,927,114]del	-	Loss
	L13 (HM15)	Not deleted, mutation NE	not deleted, mutation NE	-	-	chr11:hg19:g[84,797,189_84,797,248]_[134,927,055_134,927,114]dup	-	Positive
	L14 (HM17)	c.5839C>T; p.Arg1947*	not deleted, mutation NE	-	-	chr11:hg19:g[55,033,201_55,033,320]_[134,927,055_134,927,114]del	c.635-1G>A; splice defect	Loss
	L15 (HM19)	c.1712-1G>A; splice defect	not deleted, mutation NE	-	-	-	-	Positive
	L17 (HM22)	c.3113+1G>T; splice defect	chr17:hg19:g[28,470,078_28,470,137]_[81,124,168_81,124,227]amp	somatic chr17:hg19:g[28,470,078_28,470,137]_[81,124,068_81,124,227]amp	-	-	-	NE
	L18 (HM23) = 88-3	c.6950T>C; p.Leu2317Pro	not deleted, mutation NE	somatic c.275-46_275-2del; splice defect	somatic c.275-46_275-2del; splice defect	-	-	NE
	L2 (HM2) = S462	c.6792C>A; splice defect	chr17:hg19:g[48,539_48,598]_[81,124,183_81,124,227]del	chr17:hg19:g[48,539_48,598]_[81,124,183_81,124,227]del	-	-	-	NE
	L20 (HM25)	Not deleted, mutation NE	chr17:hg19:g[26,152,112_26,152,171]_[31,336,208_31,336,267]del	somatic chr17:hg19:g[26,152,112_26,152,171]_[31,336,208_31,336,267]del	-	chr11:hg19:g[55,050,707_55,050,766]_[134,927,055_134,927,114]del	-	Loss
	L21 (HM26)	-	not deleted, mutation NE	-	-	-	-	Positive
	L22 (HM28)	c.760+1T; p.(Gly26*)	not deleted, mutation NE	-	-	-	-	Positive
	L23 (HM30)	Not deleted, mutation NE	not deleted, mutation NE	-	-	-	-	Positive
	L6 (HM6)	Not deleted, mutation NE	not deleted, mutation NE	-	-	-	-	Loss
	P12	c.5839C>T; p.Arg1947*	c.2340T>C; p.Leu847Pro	-	-	chr11:hg19:g[85,597,254_85,600,644]_[86,940,763_86,947,630]del	chr11:hg19:g[85,597,254_85,600,644]_[86,940,763_86,947,630]del	pLoss
	P13	c.1885G>A; p.Gln616Gly*4	-	-	-	-	-	NE
	P14	-	-	-	-	-	-	Loss
	P15	c.889-2A>G; splice defect	CN-LOH (including *NF1* + *SUZ12*)	somatic CN-LOH (including *NF1* + *SUZ12*)	somatic c.1564A>T; p.(Arg522*)	-	-	NE
	P17	Not deleted, mutation NE	NE	-	-	c.726T>C; p.(Ala242Ala)	c.726T>C; p.(Ala242Ala)	NE
	P19	c.1039C>T; p.(Gln347*, Lys297_Lys354del]	CN-LOH (including *NF1* + *SUZ12*)	somatic CN-LOH (including *NF1* + *SUZ12*)	somatic c.732dup; p.(Met244Ilefs*10)	-	-	NE
	P20	c.4204_4205delinsCAT; p.(Glu1402Hisfs*7	chr17:hg19:g[22,218,445_25,375,449]_[35,745,659_35,754,684]del	somatic chr17:hg19:g[22,218,445_25,375,449]_[35,745,659_35,754,684]del	-	chr11:hg19:g[85,944,362_85,952,771]_[86,336,477_86,341,086]del	chr11:hg19:g[85,944,362_85,952,771]_[86,336,477_86,341,086]del	NE
	P3	chr17:hg19:g[29,484,390_29,485,231]_[29,493,102_29,493,220]del	CN-LOH (including *NF1* + *SUZ12*)	somatic CN-LOH (including *NF1* + *SUZ12*)	somatic c.1671_1672dup; p.(Ser558Ilefs*25)	-	-	Loss
	P4	c.3G>T; p.Met1?	c.2525del; p.(Gly842Alafs*36)	-	-	-	-	pLoss
	P6	c.2953C>T; p.Gln985*	c.6789_6792del; p.Tyr2267Thrfs*5	-	-	-	-	Positive
	P8	c.2323T>C; p.(Trp777Arg)	-	-	-	-	-	Positive
	P9	c.1986del; p.(Asn664Thrfs*24)	-	-	-	-	-	Positive

NE: not examined
-: not detected
CN-LOH: copy neutral LOH
MD: microdeletion
pLoss: partial loss
NF1: chr17:hg19:g[29,421,945_29,709,134]
SUZ12:chr17:hg19:g[30,264,037_30,328,064]
EED:chr11:hg19:g[85,955,586_85,989,778]
yellow: Full inactivation
light green: heterozygous loss

Mutations and resulting amino-acid changes in *NF1*, *SUZ12* and *EED* are shown. H3K27me3 staining results, when performed, are indicated and tumours are classified as strongly positive, negative (loss) or partial loss (ploss). The majority of MPNSTs harbour defects in the p53 pathway.